Liquid Crystals
Publication details, including instructions for authors and subscription information:
http://www.informaworld.com/smpp/title~content=t713926090

Torques and textures from capillary flow of cholesteric liquid crystals

L. Thesing[a]; F. Fischer[a]
[a] Physikalisches Institut, Westfälische Wilhelms-Universität, Münster, F. R. Germany

To cite this Article Thesing, L. and Fischer, F.(1990) 'Torques and textures from capillary flow of cholesteric liquid crystals', Liquid Crystals, 7: 1, 81 — 94
To link to this Article: DOI: 10.1080/02678299008029195
URL: http://dx.doi.org/10.1080/02678299008029195

LIQUID CRYSTALS, 1990, VOL. 7, NO. 1, 81–94

Torques and textures from capillary flow of cholesteric liquid crystals

by L. THESING and F. FISCHER
Physikalisches Institut, Westfälische Wilhelms-Universität, Münster, F.R. Germany

(*Received 8 May 1989; accepted 4 August 1989*)

The torque effect of low twist cholesterics on capillary axial flow between coaxial cylinders has been studied as a function of flow rate and pitch. The motion of disclinations and textures as well as the flow-induced transformation into new textures were separately studied. A model of simultaneous translational flow (of Poiseuille type) and permeation describes the experimental relations in a quantitative way. Maximum permeation of about 2 per cent of total flow was found for a pitch being near the thickness of capillary layer.

1. Introduction

Recently we have reported a new torque effect for cholesterics undergoing capillary flow between coaxial cylinders [1]. The axial flow in the vertical direction generates a mechanical torque upon the inner cylinder suspended on a thin filament of silica. We interpreted this torque in terms of the action of a special kind of flow termed and depicted by Helfrich [2] as permeation. Here a macroscopic flow of the cholesteric takes place along its own texture and the director rotates around the local permeation velocity $\mathbf{v}_p$. As in the Tsvetkov effect [3] caused by an external rotating magnetic field, we observe the transfer of torque to the walls. While in the Tsvetkov case the anti torque acts upon the rotating magnet, in our experiment two separate coaxial cylinders are required to fulfil the conditions of action = reaction.

In our note [1] we reported on results obtained from MBBA (4-methoxybenzylidene-4′-*n*-butylaniline) doped with 3·13 wt % CC (cholesteryl chloride) concerning the flow-induced rotation of the torsional pendulum of the inner cylinder. We measured its angular velocity at zero passage $\dot{\Phi}$, the stationary maximum angle Φ_m, and the volume flow rate Q as a function of the pressure difference Δp between the capillary ends. For sufficiently small $|\Delta p|$ we obtained $\dot{\Phi} \sim \Delta p$, $\Phi_m \sim \Delta p$, and $Q \sim \Delta p$. In this paper instead of Δp we use Q as a free parameter and we shall determine the functional dependencies $\dot{\Phi}(Q)$ and $\Phi_m(Q)$. Our main effort is directed at the influence of the cholesteric pitch for various mixtures of MBBA with CC or CB15, respectively. Independent optical studies of textures under comparable conditions of cell dimension and flow rates were performed in order to learn more about the stability of the textures against flow at low Q. We shall report on drift velocities of textures and disclinations; transformations of textures are also observed. Finally the optical and mechanical data are compared and discussed.

2. Experimental details

2.1. *Construction of the torque device*

Figure 1 (*a*) gives a cross sectional view of the torque cell made out of stainless steel. A solid cylinder (radius $R_1 = 2{\cdot}90$ mm; height $h = 10$ mm) is suspended on a

0267-8292/90 $3.00

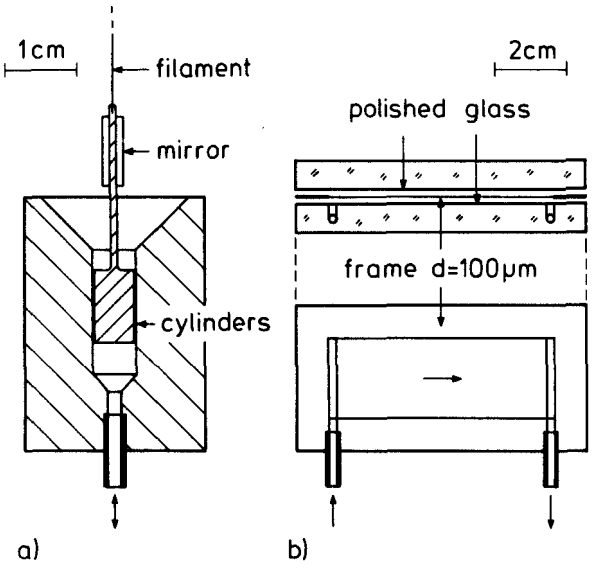

Figure 1. Sketch of the torque cell (*a*) and the optical cell (*b*).

30 μm and 31 cm long filament of silica and forms a torsional pendulum with directional constant $D^* = (7{\cdot}40 \pm 0{\cdot}07) \times 10^{-9}$ Nm/rad. The total inertial mass I consisting of contributions from the cylinder, a thin coaxial pin, and two surface mirrors, glued to the pin, has been calculated from the known shape and density of the different parts. The second mirror is used mainly for levelling. From the measured period of oscillation T we find $D^* = 4\pi^2 I/T^2$. With a telescope we observe over one mirror a linear scale illuminated from behind. The distance of 1·85 m between scale and rotational axis, together with the scale value, allows us to obtain the instantaneous orientation of the inner cylinder over an angular range of 300 mrad (17°) with an accuracy of 0·3 mrad. The orientation of the relaxed free pendulum is used as the zero point of our angular scale.

An external hollow cylinder ($R_2 = 3{\cdot}00$ mm) forms a capillary channel of width $d = R_2 - R_1 = (100 \pm 5)\,\mu$m with the inner cylinder. This requires careful vertical adjustment with a spirit-level of the axis of the external cylinder, mounted on a base plate. The upper suspension of the silica filament can be shifted horizontally by two micrometer screws acting normal to one another. Mutual contact of both cylinders causes strong damping. This observation allows accurate centring of the inner cylinder. The entire upper suspending device rests on top of a glass tube at the base plate of the torque device. This tube protects the torque balance against air motions. In order to avoid distortion of the optical beam a plane window replaces the bent glass of the tube in front of the mirror.

A motor driven microlitre syringe (Glenco) feeds the liquid crystal from below to the torque cell. A definite DC voltage provides the required volume flow rate Q which can be chosen between 10^{-11} and 2×10^{-9} m^{3}s^{-1}. Because of the limited volume of the syringe (100 mm^3) the flow has to be reversed regularly. In our convention positive Q means flow from below.

High-polish of both cylinders is very important. Certainly coil-shaped traces from the lathe-working are not allowed. Indeed they could lead to torque effects even with

isotropic liquids. After careful polishing of the relevant surfaces on the lathe no torque effect was found in tests with ethanol or pure MBBA. An irregularly varying drift of Φ, without flow occurring gives $|\dot{\Phi}| \leqslant 40\,\mu\text{rad}\,\text{s}^{-1}$ which can be neglected compared to the measured effects. In our convention positive $\dot{\Phi}$ means rotation of the inner cylinder in a clockwise direction when viewed from above. The cholesterics we have used are either MBBA doped with CC [4] or MBBA doped with CB 15 (4-cyano-4′-2-methylbutylbiphenyl) [5] having left ($P < 0$) or right ($P > 0$) handed helices, respectively. The pitch P of each mixture was measured by the Cano wedge method [6, 7]. The largest values were approximately 200 μm; values of the helical twist $q_0 = 2\pi/P$ cover the range $-1{\cdot}2\,\mu\text{m}^{-1}$ to $+1{\cdot}6\,\mu\text{m}^{-1}$.

2.2. *The device for optical studies of flowing textures*

Figure 1 (*b*) gives a schematic view of the plane flow device used in this investigation. It allows us to observe textures of the cholesterics under similar conditions of flow as in the torque cell. Two thick plane polished glass plates replace the cylinder walls. A frame cut from a mylar foil provides the same thickness d of 100 μm. Into the lower glass plate bore holes and grooves are worked with diamond tools. They serve as inlet and outlet of the liquid crystal which is supplied by the same microlitre syringe used for the torque device. The width of the flow channel, b, is 23·0 mm, which is a little larger than the corresponding width, $2\pi R$, of 18·5 mm for the torque device. This provides comparable situations in both devices at the same flow rates. The time-dependent textures are observed under a polarizing microscope and can be documented by a camera. At the state of present investigation there are still two differences between both flow experiments which concern the boundary conditions. The glass plates have been covered with lecithin, to obtain homeotropic alignment at the surfaces; in this way we obtain a clearly arranged fingerprint texture. No lecithin was applied to the cylindrical surfaces. Whereas the glass plates are mutually fixed the inner cylinder can rotate and causes additional simple shear flow until the maximum torsion is reached at Φ_m.

3. Results from the torque experiments

After filling the torque device with liquid crystal the torsional pendulum shows overcritical damping of its rotational motion. The inertial term $I\ddot{\Phi}$, therefore, has been neglected in the equation of motion

$$\Gamma\dot{\Phi} + D^*\Phi = M. \tag{1}$$

The frictional parameter Γ, calculated for cylindrical symmetry, is

$$\Gamma = 2\pi\eta_{\text{eff}}R^3h/d, \tag{2}$$

where η_{eff} is an effective viscosity parameter which depends on the present texture and therefore is a function of previous events, flow rate, and time. Three special modes of measurement are used in our experiments. In the first case we measure $\dot{\Phi} = \Delta\Phi/\Delta t$ near $\Phi = 0$ at constant flow rate. Here we may neglect $D^*\Phi$ and retain $\dot{\Phi} = M/\Gamma$. A direct comparison with the torque expected from plug flow (pure permeation), however, is not feasible while η_{eff} is unknown. In the second case we measured the stationary maximum angle Φ_m at constant flow rate as $\Phi_m = M/D^*$. In the third case we investigate the relaxational angular motion at $Q = 0$ of the inner cylinder. Its analysis allows a detailed study of η_{eff}; moreover we learn about the certain hysteretic behaviour of Φ.

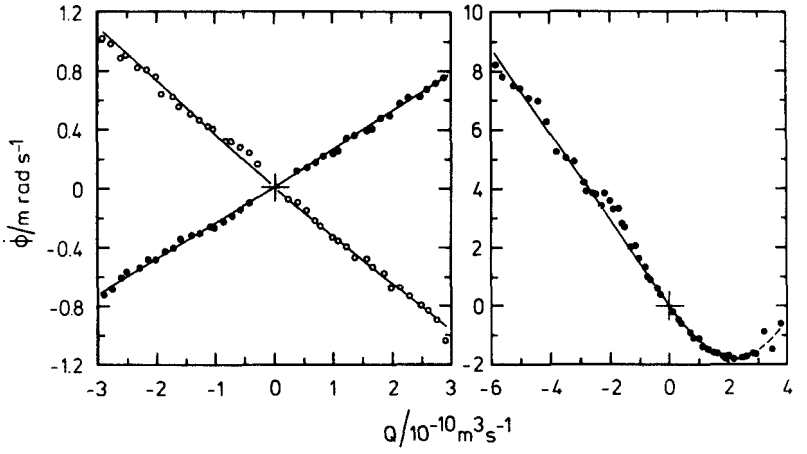

Figure 2. The angular velocity at zero passage, $\dot{\Phi}$, versus flow rate, Q, of MBBA mixtures. Left: ○, CC (0·83 wt %, $P = -15{\cdot}1 \pm 0{\cdot}8$ mm); ●, CB15 (0·59 wt %, $P = 13{\cdot}6 \pm 0{\cdot}5\,\mu$m). Right: CC (0·12 wt %, $P = -99 \pm 5\,\mu$m).

We consider first the dependence of the angular velocity $\dot{\Phi}$ on the flow rate Q. Figure 2(*a*) shows, for two examples, the strong proportionality between $\dot{\Phi}$ and Q and the different signs of $m = \dot{\Phi}/Q$ for left and right handed helices of MBBA : 0·83 wt % CC and MBBA : 0·59 wt % CB15, respectively. The data points have been collected with alternating signs and increasing absolute values of Q. Aging effects require prompt measurements on freshly prepared samples. On the less doped MBBA : 0·12 wt % CC with $P = (99 \pm 5)\,\mu$m the straight course was followed down to $Q = -6 \times 10^{-10}\,m^3\,s^{-1}$ (see figure 2(*b*)). For $Q > 0$, however, the data points trace a minimum and begin to scatter at higher Q. We suppose an instability of the inner cylinder due to a compensation of its weight by buoyancy and the additional lifting force $\pi R^2 \Delta p$. The straight line for $Q < 0$ shows the average course of the data points. Their deviations, however, are not irregular but very systematic so that a more stepwise course is also possible. This could be connected with sudden, major changes in the texture. The slope $m = \dot{\Phi}/Q$ obtained for small $|Q|$ from such measurements is mainly determined by the helical pitch. This is shown in figure 3 where we have collected the data points of $|m|$ versus $|P|$ from 28 different cholesteric mixtures; the error bars mark the growing uncertainty at higher $|P|$. After a linear increase of $|m|$ with $|P|$ a bendover to saturation is indicated when $|P|$ exceeds the layer thickness d of 100 μm.

Direct measurement of a stationary maximum angle Φ_m at constant Q is only feasible for small $|Q|$ and sufficiently large $|P|$ because of the limited capacity of the microliter syringe. Therefore we use the low $Q = \pm 12 \times 10^{-12}\,m^3\,s^{-1}$ for the following experiments. The indirect determination of Φ_m by extrapolation of $\Phi(t)$ is complicated by the problem of possible changes in η_{eff}. However, by proper choice of Φ_m the difference $|\Phi_m - \Phi(t)|$ can be well adapted to an exponential trace. Table 1 lists the mixtures and the measured pitch together with the maximum angle Φ_m; two more results from higher doped samples are also included. One (with CC) is taken from equations (5) and (6) out of [1]; the other (with CB15) has been obtained by extrapolating the $\Phi(t)$ curve. A discussion of these findings will follow in the last section.

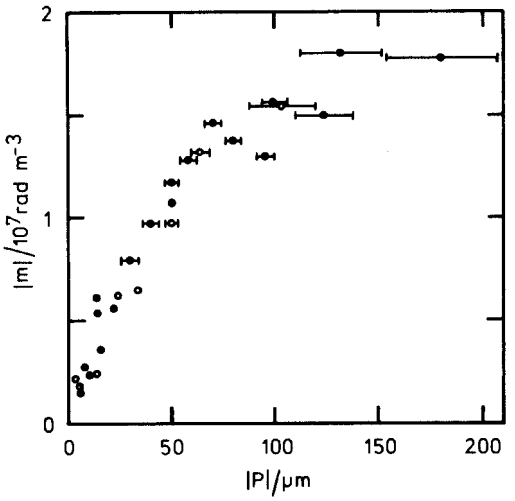

Figure 3. $|m| = |\Phi/Q|$ versus $|P|$ of MBBA doped with CC (●, $P < 0$) and CB15 (○, $P > 0$).

Table 1. Maximum angle Φ_m at constant flow rate $Q = 12 \times 10^{-12}\,m^2s^{-1}$ for various mixtures of MBBA with CC or CB15.

	Chiral additive in wt %	Pitch $P/\mu m$	Maximum angle Φ_m/mrad	x in per cent
CC	0·06	−180 ± 25	23 ± 5	1·93 ± 0·6
	0·10	−123 ± 13	30 ± 5	1·72 ± 0·5
	0·12	−99 ± 5	25 ± 5	1·15 ± 0·3
	0·16	−70 ± 4	27 ± 5	0·88 ± 0·2
	0·24	−49·4 ± 1·9	55 ± 6	1·26 ± 0·2
	3·13†	−6·1 ± 0·3†	13 ± 3†	0·04 ± 0·01
CB15	0·09	104 ± 15	35 ± 2	1·69 ± 0·4
	0·16	63·4 ± 2·3	36 ± 1	1·06 ± 0·1
	0·21	50·3 ± 1·6	54 ± 2	1·26 ± 0·1
	0·29	33·4 ± 1·2	50 ± 4	0·78 ± 0·1
	0·36	24·3 ± 1·2	46 ± 1	0·52 ± 0·06
	1·38	6·9 ± 0·3	28 ± 2‡	0·09 ± 0·01

† From [1].
‡ Extrapolated.

Finally we report on the relaxation $\Phi(t)$ of the torsional pendulum at $Q = 0$ after the previous flow has turned the inner cylinder to a large extension $\Phi(0)$. Figure 4 shows the results for MBBA/CC mixtures with various helical pitches. Obviously the pendulum moves very slowly for small-pitch mixtures. After observation for 30 min $\Phi(t)$ has reached a residual value for the two mixtures with larger P. Also the other curves seem to terminate at a residual offset angle Φ_R, which is higher the smaller is P. We understand this behaviour as a typical hysteresis phenomenon. When subtracting a proper Φ_R we obtain in figure 5 the logarithmic plot of $|\Phi(t) - \Phi_R|$ versus time, t, as a straight line for each relaxation course shown in figure 4. Data for the first one to two minutes where we observe a faster relaxation than given by the slope of the respective straight lines are excluded; this deviation will be discussed later. In table 2

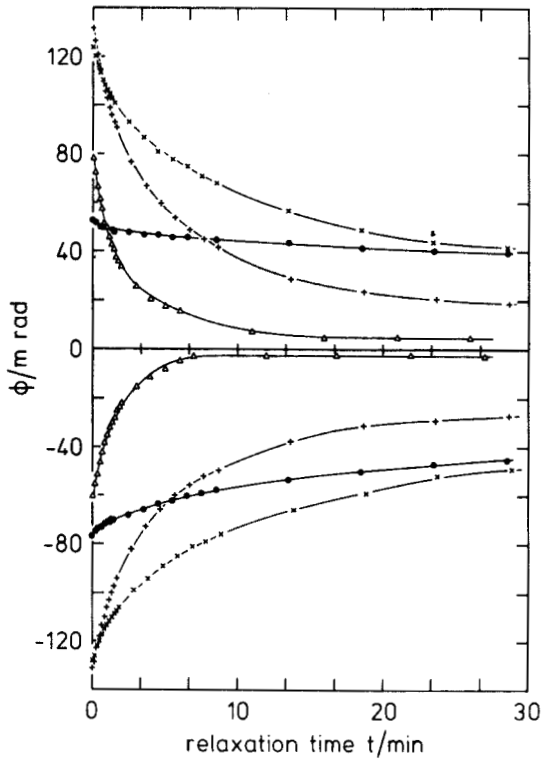

Figure 4. Relaxation of the angle Φ with time, t, after torsional extension by flow of MBBA : CC. $P = -5{\cdot}3 \pm 0{\cdot}1\,\mu$m (●), $P = -13{\cdot}6 \pm 0{\cdot}4\,\mu$m (x), $P = -39{\cdot}2 \pm 2{\cdot}5\,\mu$m (+), $P = -96{\cdot}9 \pm 2{\cdot}5\,\mu$m (△).

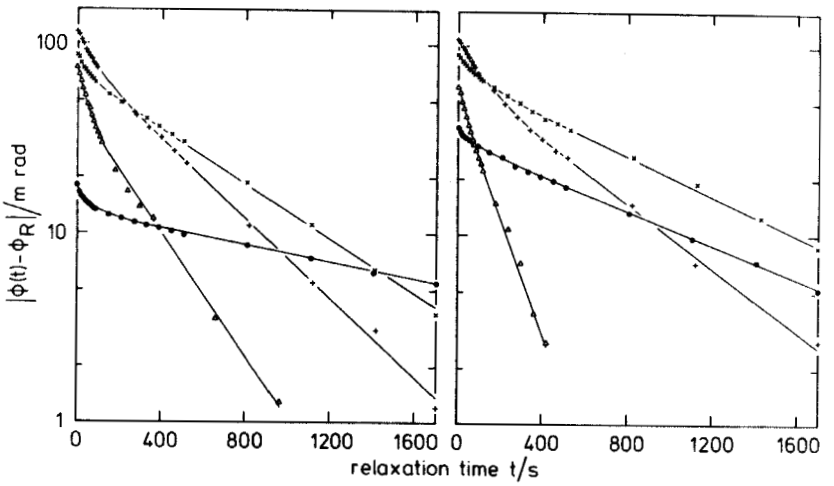

Figure 5. $|\Phi(t) - \Phi_R|$ versus time, t (Φ_R residual angle). Left (right) for $\Phi(0) > 0 (\Phi(0) < 0)$. $P = -5{\cdot}3 \pm 0{\cdot}1\,\mu$m (●), $P = -13{\cdot}6 \pm 0{\cdot}4\,\mu$m (x), $P = -39{\cdot}2 \pm 2{\cdot}5\,\mu$m (+), $P = -96{\cdot}9 \pm 2{\cdot}5\,\mu$m (△).

Table 2. Relaxation of $\Phi(t)$ without torque. Residual angles Φ_R and relaxation times τ for MBBA : CC mixtures with different helical twist $q_0 = 2\pi/P$.

		Φ_R/mrad		τ/s	
Pitch $\lvert P\rvert/\mu$m;	$\lvert q_0\rvert$/mm^{-1}	$\Phi(0) > 0$	$\Phi(0) < 0$	$\Phi(0) > 0$	$\Phi(0) < 0$
5·3 ± 0·1	1186	35	−42	2270	940
13·2 ± 0·8	476	36	−65	750	760
13·6 ± 0·4	462	38	−40	600	850
30·5 ± 1·3	206	41	−42	690	680
39·2 ± 2·5	160	18	−24	400	530
57·8 ± 3·2	109	20	−22	680	790
79·6 ± 3·5	79	13	−12	530	490
96·9 ± 2·5	65	4	0	300	140

we have collated the offset angles Φ_R and the relaxation times τ of the exponential part together with the pitch P and q_0 for all of the samples and curves measured and analysed by us. Apart from one case all of the data points for $q_0 > 200\,\text{mm}^{-1}$ give $|\Phi_R| \approx 40$ mrad which means a kind of saturation in the residual. For smaller q_0 we observe a strong decrease in Φ_R which may become zero for $P > d$. Values of τ tend to decrease with increasing pitch, more strongly near $P = d$.

4. Results from optical studies

After filling the optical flow cell with MBBA : 0·59 wt % CC a typical finger-print texture is formed within one hour. Compared to the pitch P of 21·8 ± 0·6 μm measured in a Cano wedge the fingerprints in the 100 μm thick cell have a period of 103 ± 3 μm. Domains with the helical axis normal and parallel to the flow direction are preferred. In figures 6 and 7 we have selected ranges of relatively large domains, 5·7 mm × 1·9 mm, with such uniform orientations. Compared to the total area, however, they are still small and globally disorder prevails. The average flow velocity $\bar{v}$ of 5·0 ± 0·8 μm s^{-1}, calculated from $\bar{v} = Q/bd$, corresponds to $Q \approx 10^{-11}$ m^3 s^{-1} in the cylindrical cell. With the initial orientation of the helical axis normal to the flow direction (see figure 6) the texture is completely changed as soon as the flow is started. Figures 6 (*b*) and (*c*) are pictures taken after 7 and 15 min, respectively, of the same section as in figure 6 (*a*). The whole area of uniform fingerprint texture is transformed into a rhombic pattern with only a faint contrast. Small ranges of differently oriented textures, mixed with disclinations and dislocations, which travel with the flow are unchanged. Shortly after the picture in figure 6 (*c*) was taken we stopped the flow; figure 6 (*d*) shows the same range 2 min later. While the other textures and defects remain unchanged we observe a strong increase of contrast in the rhombic domain. One hour later the rhombic domain has disappeared and the old fingerprint texture with its former orientation was nearly reestablished.

The same flow rate turned out to cause quite different results when the helix axis was parallel to the flow direction (see figure 7). The fingerprint texture remains stable against flow while increasing its contrast and line defects also appear sharper. We observe that the drift velocity for disclination loops (v_D) is higher than for fingerprints (v_F). We have performed systematic measurements of such velocities using MBBA : 0·82 wt % CC in a 100 μm thick cell and MBBA : 0·31 wt % CC in a thicker cell ($d = 180\,\mu$m). In figure 8 the relative velocities

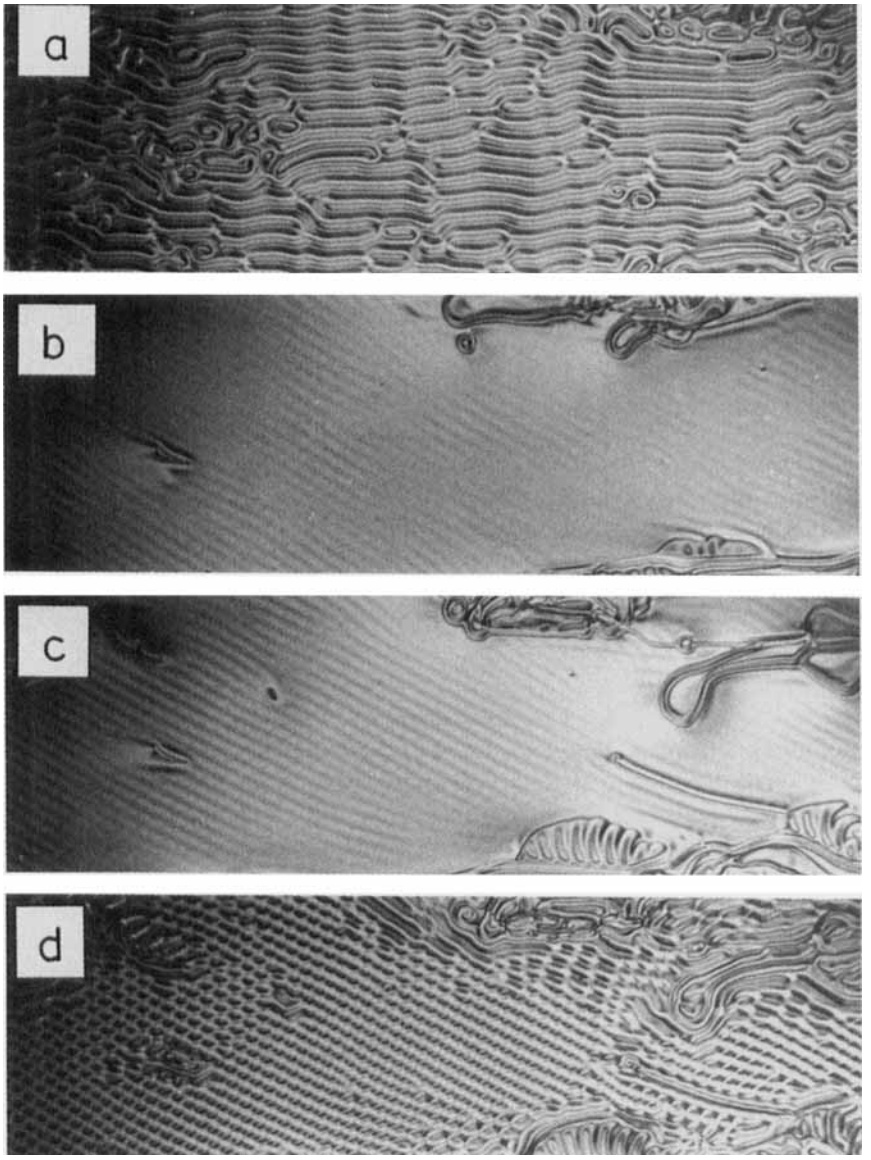

Figure 6. The fingerprint texture (sectional view) with the helical axis normal to the flow velocity (right to left. MBBA: 0·59 wt % CC, $P = 21{\cdot}8 \pm 0{\cdot}6\,\mu$m, $d = 100\,\mu$m, $\bar{v} = 5{\cdot}0 \pm 0{\cdot}6\,\mu\text{ms}^{-1}$). Top to bottom: Before flow starts (*a*), 7 min (*b*), and 15 min after flow starts (*c*), 2 min after flow stops again (*d*).

$v_F/\bar{v}$ and $v_D/\bar{v}$ are plotted versus $\bar{v}$. Within the error limits these ratios are constant and independent of $\bar{v}$. However, $v_F/\bar{v}$ can only be measured up to $\bar{v} = \bar{v}_m$ because the fingerprints have disappeared above $\bar{v}_m$. While $v_D/\bar{v}$ is also found to be independent of the pitch namely $v_D/\bar{v} = 1{\cdot}56 \pm 0{\cdot}12$, we obtain $v_F/\bar{v}$ as a function of P as shown in figure 9. For both cell thicknesses d we obtain a linear increase of $v_F/\bar{v}$ with P. The ratio extrapolated to zero P is definitely different from zero. Against higher P values the range is limited because fingerprints are

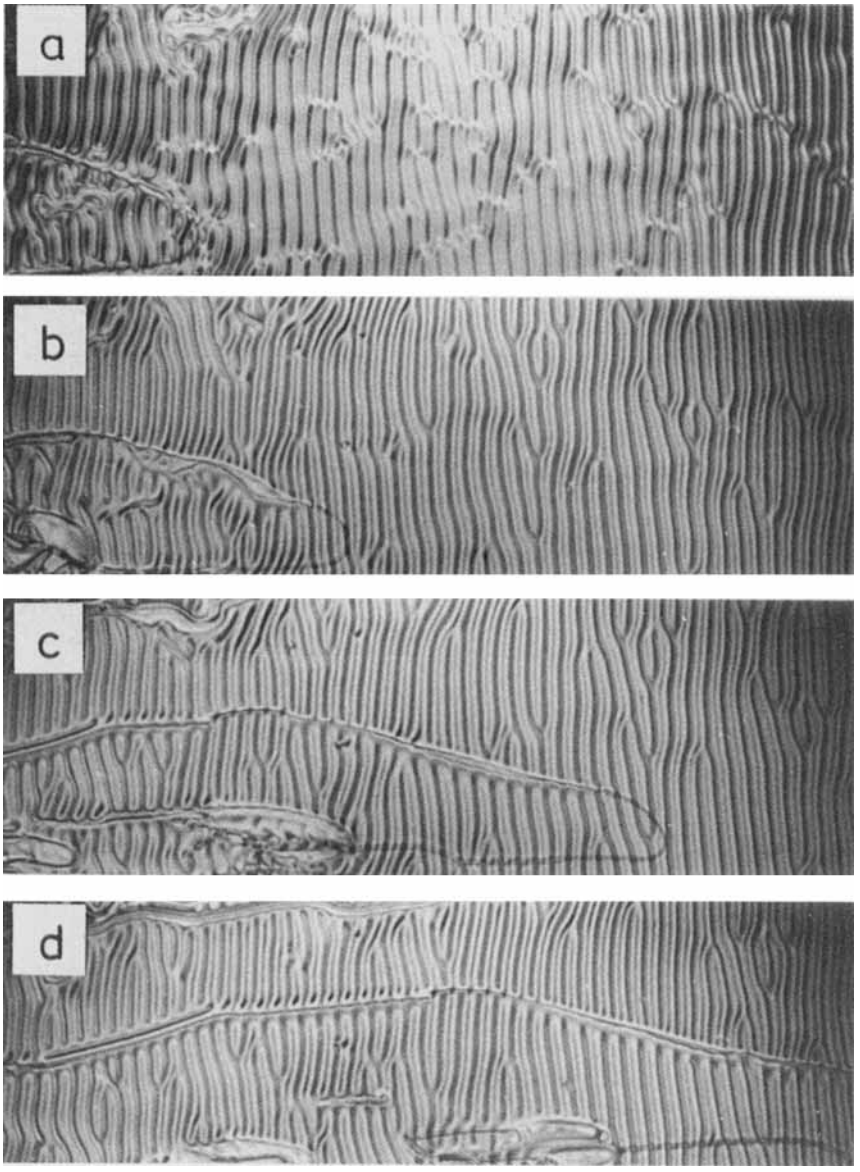

Figure 7. The fingerprint texture (sectional view) with the helical axis parallel to the flow velocity (left to right, MBBA 0·59 wt % CC). Top to bottom: Before flow starts (*a*), 2 min (*b*), 6 min (*c*), and 10 min (*d*) after flow starts.

finally transformed into a homeotropic texture without any structure. As already known from figure 8 by increasing the pitch the range of stable fingerprints is reduced to smaller and smaller $\bar{v}$.

In figure 10 the maximum average flow velocity $\bar{v}_m$, at which the determination of v_F is even feasible, has been plotted as a function of q_0 $(2\pi/P)$. The linear extrapolation of the data points cuts the abscissa at q_0 of $5 \times 10^4\,m^{-1}$ for d of 180 μm. For q_0 values below this limit the homeotropic texture should already be stable without flow.

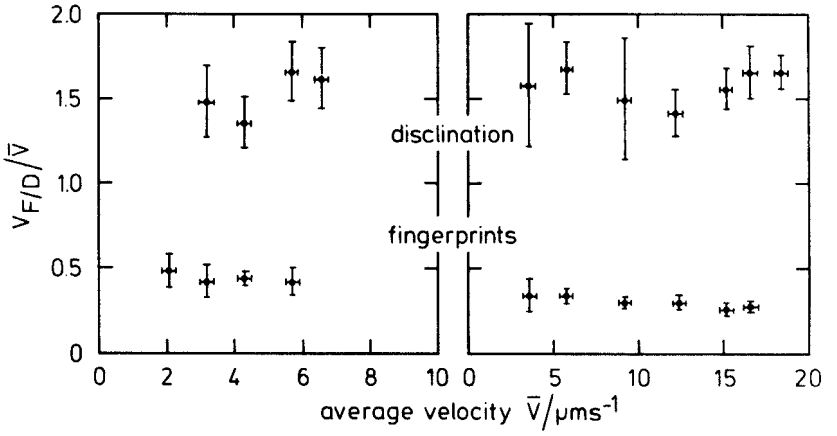

Figure 8. Ratio of v_D (disclination) and v_F (finger prints) over the average velocity $\bar{v}$ versus $\bar{v}$. Left: Cell thickness $d = 180\,\mu m$, MBBA: 0·31 wt % CC, $P = 37{\cdot}2 \pm 0{\cdot}9\,\mu m$. Right: $d = 100\,\mu m$, MBBA: 0·82 wt % CC, $P = 17{\cdot}7 \pm 0{\cdot}4\,\mu m$.

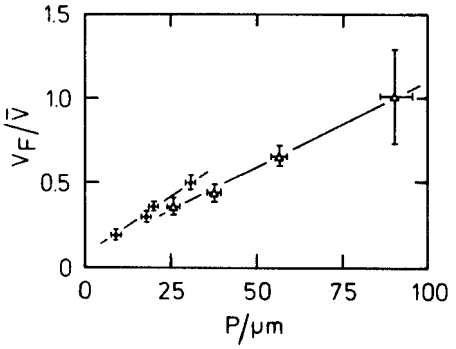

Figure 9. $v_F/\bar{v}$ averaged over data taken at different $\bar{v}$ as a function of P. MBBA: CC, $d = 180\,\mu m$ (△), $100\,\mu m$ (●).

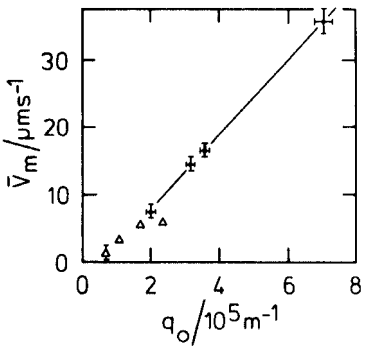

Figure 10. Maximum average velocity $\bar{v}_m$ for stable fingerprint texture (the helical axis parallel to the velocity) as a function of the helical twist $q_0 = 2\pi/p$. MBBA: CC, $d = 180\,\mu m$ (△), $d = 100\,\mu m$ (●).

A corresponding $\bar{v}_m$ for the helical axis normal to the flow direction should also exist but be expected at less than $5\,\mu m\,s^{-1}$ ($Q < 10^{-11}\,m^3\,s^{-1}$). Present limitation in obtaining lower Q, however, did not allow such measurements.

5. Discussion and conclusions

A comparative discussion of the results gained from our optical and torque measurements requires comparable conditions under which both experiments have been performed. The ratio P/d runs from 0·1 to 0·9 (0·04 to 1·8) in optical (torque) studies as can be seen from figures 9 and 10 (3), respectively. The Q values in our optical (torque) experiments are less than $8 \times 10^{-11}\,m^3\,s^{-11}$ (between 2·2 and $60 \times 10^{-11}\,m^3\,s^{-1}$) as shown in figures 6, 7, 8, and 10 (2), respectively. The overlap is sufficient to allow a direct comparison so that we have to suppose that above about $8 \times 10^{-11}\,m^3\,s^{-1}$ all fingerprint textures are destroyed.

The constancy of $v_D/\bar{v}$ (see figure 8) against variations in $\bar{v}$ and P, as well as its magnitude ($\sim 1{\cdot}5$) could mean a kind of Poiseuille flow with a parabolic distribution of local velocities across the capillary. The disclination prefers the middle part of the cholesteric layer and data scattering is influenced by the different curvatures of the disclination loops studied. The very low values of $v_F/\bar{v}$ (down to 0·2) shown in figure 9 could let us suppose that with decreasing pitch an increasing portion of flow takes place through permeation. This, however, contradicts the independence of $v_D/\bar{v}$ on P. Instead we believe in a gradual pushing aside of the fingerprint rolls against the walls. The disappearance of the fingerprint texture (see figure 10) is a continuous process towards the unknow flow induced texture, which can not mean a first order transition. More as a first order phase transition has to be seen the destruction of fingerprints with their helical axis normal to the flow direction caused already by the smallest flow rates ($Q = 12 \times 10^{-12}\,m^3\,s^{-1}$) as shown in figure 6. The growing contrast of the rhombic texture (centred rectangular lattice, $a = 83\,\mu m$, $b = 135\,\mu m$), after the flow was stopped, means the stabilization of this (now) metastable texture,

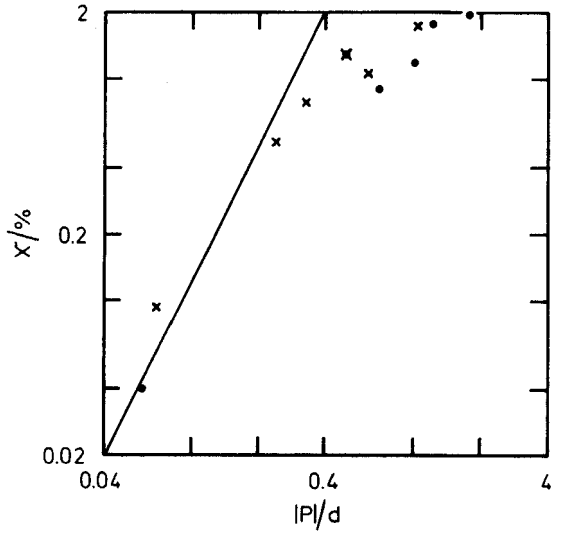

Figure 11. Relative contribution of permeation $x = v_p/\bar{v}$ as a function of $|P|/d$. Straight line (slope 2) from equation (10); (●) CC and (x) CB15.

while the slow transformation back to the fingerprints starts from the boundaries of this domain.

Let us now introduce a model which allows us to interpret the torque results in a more detailed way. In the relation

$$Q = 2\pi R d\bar{v}, \tag{3}$$

we assume that $\bar{v}$ consists of two additive contributions

$$\bar{v} = v_p + v_t \tag{4}$$

of velocities v_p of permeation and v_t of translation meaning a kind of Poiseuille flow, and both averaged over the layer thickness and over the whole layer area. We define

$$x = v_p/\bar{v} \tag{5}$$

as the relative contribution of permeation to the total flow. In advance we note that x comes out to be less than 2 per cent, which means $v_t \approx \bar{v}$ in all of our experiments.

From the hydrodynamic equations given by Leslie [8], applied to the simple plug flow or as described by Helfrich [2], v_p grows proportional to the pressure gradient p'

$$p' = |\lambda_1| q_0^2 v_p. \tag{6}$$

Here λ_1 is the viscosity coefficient for director rotation and $q_0 = 2\pi/P$ is the helical twist. The torque M acting on the torsional pendulum, which is produced by permeation, has been calculated as

$$M = |\lambda_1| q_0 v_p V, \tag{7}$$

where $V(=\pi R^2 h)$ is the cylinder volume. Macroscopic circulation of the liquid crystal around the inner cylinder can be excluded. We assume that equation (7) can be applied also in cases where $x < 1$. By using $M = D^* \Phi_m$ combined with equation (5) we obtain

$$\frac{\phi_m}{Q} = \frac{|\lambda_1| \pi R h}{D^* d} \frac{x}{P}. \tag{8}$$

From table 1 and with $|\lambda_1| = 0{\cdot}143$ s Pa for pure MBBA [9] all data except x are known. So we are able to calculate x and we find all x are less than 2 per cent (see table 1). Figure 11 provides a double logarithmic plot of all x versus $|P|/d$. The straight line with slope two expresses a functional relation $x \sim P^2$ which is expected on theoretical grounds. Namely, by calculating Poiseuille flow simultaneously taking place with the same pressure gradient p' which causes permeation in equation (6), we obtain

$$p' = \eta_{app} \frac{12 v_t}{d^2}, \tag{9}$$

with η_{app} being an effective viscosity different from η_{eff} in equation (2). From equations (6) and (9) we obtain

$$x = \frac{3}{\pi^2} \left| \frac{\eta_{app}}{\lambda_1} \right| \cdot \left(\frac{P}{d} \right)^2 \tag{10}$$

and so we find that x is a function only of the ratio of P/d. The straight line in figure 11 gives $\eta_{app} \approx 0{\cdot}06$ s Pa which fits well with viscosity data of MBBA [10]. The

deviation of the measured x values from the square law at higher P/d becomes large above the critical $(P/d)_c = 2K_2/K_3 \approx 0{\cdot}7$ [11] which holds for homeotropic boundaries. For very large P/d we expect x to drop again. So maximum x should not be much higher than 2 per cent. The question if and how x could be increased is kept open.

The relations obtained so far also allow us to formulate the ratios of experimental data given in [1]. With $p' = \Delta p_0/h$ in equation (6) and $M = \Gamma\dot{\Phi}$ in equation (7) we derive

$$\frac{\dot{\Phi}}{\Delta p_0} = \frac{Pd}{4\pi\eta_{\text{eff}}Rh}. \tag{11}$$

With equation (9) and equation (3) we obtain

$$\frac{Q}{\Delta p_0} = \frac{\pi Rd^3}{6\eta_{\text{app}}h} \tag{12}$$

and with $M = D^*\Phi_m$ we conclude from equations (6) and (7) that

$$\frac{\Phi_m}{\Delta p_0} = \frac{R^2p}{2D^*}. \tag{13}$$

The slope $m = \dot{\Phi}/Q$ plotted in figure 2 can immediately be found from equations (11) and (12) as

$$m = \frac{3}{2\pi^2}\left(\frac{\eta_{\text{app}}}{\eta_{\text{eff}}}\right)\frac{P}{R^2d^2}. \tag{14}$$

So we verify $|m| \sim |P|$ found for small $|m|$. The experimental slope of $2{\cdot}6 \times 10^{11}\,\text{rad m}^{-4}$ compared to m/P from equation (14) gives $\eta_{\text{eff}} = 6{\cdot}5\,\eta_{\text{app}}$ and using $\eta_{\text{app}} \approx 0{\cdot}06\,\text{s P}$, already determined, we obtain $\eta_{\text{eff}} \approx 0{\cdot}39\,\text{s Pa}$. However, η_{eff} can also be calculated by using τ values from table 2 together with equation (2). From $\tau = \Gamma/D^*$ we obtain

$$\eta_{\text{eff}} = \frac{D^*d\tau}{2\pi R^3h} \tag{15}$$

Using an average τ of 800 s for small P we find $\eta_{\text{eff}} = 0{\cdot}37\,\text{s Pa}$ in good agreement with the former value.

As seen from figure 5 the relaxation becomes purely exponential after a stage of faster relaxation within the first 90 s. We think that this is an effect of reduced shear friction due to the preceding fast flow-induced extension of the angle Φ. After the low-shear texture has ben reestablished we find a constant viscosity η_{eff}.

The hysteresis observed in figure 4 could be caused by a disclination (and dislocations) carried into the capillary zone during the preceding fast flow. If such a line defect is strongly anchored at both cylindrical boundaries it can be elongated and oriented during the subsequent slow relaxation of the torsional pendulum. This develops a torque which finally prevents the pendulum from reaching zero orientation.

At the end we calculate the shear rates appearing on Poiseuille flow and on torsional motion of the inner cylinder. In the latter case we have $\dot{\gamma}_T = \dot{\Phi}R/d$; in the Poiseuille case we use the maximum shear rate at the boundaries: $\dot{\gamma}_P = 3Q/\pi Rd^2$. So the ratio $\kappa = \dot{\gamma}_T/\dot{\gamma}_P$ which is only of interest here comes out to

$$\kappa = \frac{1}{2\pi}\left(\frac{\eta_{\text{app}}}{\eta_{\text{eff}}}\right)\frac{P}{d} \tag{16}$$

after $\dot{\Phi}/Q$ has been used from equation (14). An estimate for small P gives $\kappa \approx 240\,\mathrm{m}^{-1} \cdot P$, with $\kappa = 2{\cdot}4$ per cent (2·4 per mille) for $P = 100\,\mu\mathrm{m}$ (10 μm), respectively. We see that torsional shear rate is smaller by two to three orders than the shear rate of the simultaneous flow.

These investigations have been supported financially by the DFG. We also recognize the help of the Merck company for providing the CB15 sample.

References

[1] FISCHER, F., and GRUPP, J., 1984, *J. Phys. Lett., Paris*, **45**, 1091.
[2] HELFRICH, W., 1969, *Phys. Rev. Lett.*, **23**, 372.
[3] TSVETKOV, V. N., 1939, *Acta Physiochim. URSS*, **10**, 555.
[4] SAEVA, F. D., and WYSOCKI, J. J., 1971, *J. Am. chem. Soc.*, **93**, 5928.
[5] From Merck (data sheet, Sept. 1. 1987).
[6] CANO, R., 1967, *Bull. Soc. Fr. Miner. Cristallogr.*, **90**, 333.
[7] KASSUBEK, P., and MEIER, G., 1969, *Molec. Crystals liq. Crystals*, **8**, 305.
[8] LESLIE, F. M., 1966, *J. mech. appl. Math.*, **19**, 357. LESLIE, F. M., 1968, *Archs ration. Mech. Analysis*, **28**, 265.
[9] KNEPPE, H., SCHNEIDER, F., and SHARMA, N. K., 1982, *J. phys. Chem.*, **77**, 3203.
[10] GÄHWILLER, C., 1973, *Molec. Crystals liq. Crystals*, **20**, 301.
[11] FISCHER, F., 1976, *Z. Naturf.* (*a*), **31**, 41.